Supporting Information

"Top" or "Bottom" Switches of a Cyclohexanone Monooxygenase Controlling the Enantioselectivity of the Sandwiched Substrate

Yujing Hu,[a, b] Jie Wang,[a] Yixin Cen,[a] He Zheng,[a] Meilan Huang,*[b] Xianfu Lin,[a] Qi Wu*[a]

Table of Contents

[a] *Department of Chemistry, Zhejiang University, Hangzhou 310027 (China). E-mail: llc123@zju.edu.cn, wuqi1000@163.com*
[b] *School of Chemistry and Chemical Engineering, Queen's University, Belfast, BT9 5AG (U.K.). E-mail: m.huang@qub.ac.uk*

† *Electronic Supplementary Information (ESI) available. See*
DOI: 10.1039/x0xx00000x

1. Methods

The $CHMO_{Acineto}$ variants were designed utilizing a rational strategy that involves structural analysis, molecular docking, molecular dynamics (MD) simulations and experimental screening.

1.1 Computational methods

Protein preparation

The crystal structure of $CHMO_{Acineto}$ is not available, so we build a homology model (named as $CHMO_{homo}$) based on the crystal structure of CHMO from *Rhodococcus* sp. strain HI-31 (PDB code: 4RG3, contained the product ε-caprolactone), which exhibits 55% sequence similarity and thus would represent the enzyme's substrate scope and degree of selectivity.[1] The CHMO mutants were generated using Discovery Studio (version 2.5).

Molecular docking

The substrate ketones were docked to the WT $CHMO_{homo}$ and the rationally designed mutants, respectively.

Molecular docking was performed using the AutoDock 4.2 suite with the Lamarckian genetic algorithm (LGA).[2] A grid box was centered on the oxygen of the C4a-peroxy group. A total of 100 LGA runs were carried out for each ligand: protein complex. The population was 300, the maximum number of generations was 27 000, and the maximum number of energy evaluations was 2 500 000. For each system analyzed, the top-ranked structure corresponds to the lowest binding energy structure of the most populated cluster with the lowest mean binding energy.

Parameter calculations

The geometries of flavin, substrate, $NADP^+$ were optimized employing the Gaussian09 program[3], using the density functional theory (DFT) method with the exchange-correlation functional B3LYP and the 6-31g(d) basis set[4]. RESP charges[5] were obtained based on the charges calculated using HF/6-31G(d) single point energy calculations. These point charges were subsequently used in the MD simulations.

Molecular dynamics

All complex systems were subsequently subjected to energy minimization and MD simulations.

The Amber MD program (AMBER14)[6] with the parm99SB[7] and GAFF[8] force fields was used. The protein complexes were soaked within a truncated octahedral box of TIP3P waters and sodium ions were added to neutralize the system. The systems were subjected to two energy minimizations, using the steepest descent and conjugate gradient algorithms. The minimized systems were subsequently slowly heated slowly from 0 to 300 K for 250 ps using the Langevin dynamics with a collision frequency of 1.0 ps^{-1}. An equilibration simulation with no harmonic restraints applied was carried out at 300 K with a *NVT* ensemble and a periodic boundary condition for a further 50 ps. A cut-off distance of 8 Å was set for non-bonded Van der Waals force while the Particle Mesh Ewald (PME) method was used to account for the long-range electrostatic interactions.[9] The SHAKE method was utilized to fix the covalent bonds associated with the hydrogen atoms within the system.[10] 20-ns production simulation was performed for the protein complex. *NPT* ensemble was used in the MD simulations with a time step of 2 fs and a randomly assigned initial velocity at 300 K and a pressure of 1 atm. For each system analyzed, MD reference structure corresponds to the lowest RMSD structure in relation to the average structure of the simulation

1.2 Experimental methods

Materials

Hot Start DNA polymerase was purchased from TOKYO (Japan); *Dpn* I was purchased from Thermo Fischer Scientific Inc. All solvents and other reagents were analytical grade and used without further purification.

Analytical methods

Gas chromatographic analyses (GC) was used to analyze the conversion and enantiomeric excess of samples, which was conducted on a Shimadzu GC-1024C chromatograph equipped with a flame ionization detector (FID) and a CP-chirasil-DEX CB 25cm×0.25cm column (Agilent). Optical rotation data were measured on a Perkin-Elmer 341 polarimeter equipped with a Na-lamp. The ^1H and ^{13}C NMR spectra were recorded using a Bruker DRX 400 NMR spectrometer (Rheinstetten, Germany) and chemical shifts were expressed in ppm and coupling constants (*J*) in Hz.

Generation of mutant libraries

CHMO gene was obtained from Acinetobacter *sp*. NCIMB 9871 and synthesized by Sangon BioTech (Shanghai). The gene was subcloned into pET-22b (+) using Nde I and BamH I cutting sites.[11] PCR was performed using CHMO gene as the template for mutagenesis. Table S1 (Supporting Information) provides the oligonucleotide primers used for the generation of mutant libraries. PCR mixtures (50 μL final volume) contained: ddH_2O (25 μL), 10KOD buffer (5 μL), $MgSO_4$ (3 μL, 25 mM), dNTP (5 μL, 2 mM each),

forward and reverse primers (5 μL, 2.5 μM each), template plasmid (1 μL, 50 ng.μL^{-1}) and 1 μL of KOD Hot Start DNA polymerase. The PCR was initially subjected to 94 °C for 5 min, followed by 18 cycles of denaturing step at 94 °C for 1 min, annealing at 60 °C for 1 min and elongation at 72 °C for 8 min. And final extension step at 72 °C for 10 min was performed. To ensure the elimination of template plasmid, PCR mixtures were digested at 37 °C overnight after adding 2 μL *Dpn* I (10 U/μL). The digested product was purified with an Omega PCR purification spin column, and then an aliquot of 20 μL was used to transform electrocompetent *E.coli* BL21 (DE3) cells. The transformation mixture was shaken with 1 mL of LB medium at 37 °C for 1h, and spread on LB-agar plates containing 100 μgmL^{-1} ampicillin.

Expression of CHMO$_{Acineto}$ variants and the whole cell screening process

Single colony was picked into 5.0 mL LB media with 100 μgmL^{-1} ampicillin, and then incubated at 37 °C under shaking of 200 rpm for 12h. After DNA sequencing, the target mutants were conserved at -80 °C with 30% glycerol aliquot. A fresh 20.0 mL of TB media in 50mL erlenmeyer flasks containing 100 μgmL^{-1} ampicillin mixed with 200 μL preculture was inoculated at 37 °C, 200 rpm until the OD_{600} reached between 0.6 and 0.7. Then isopropyl β-thiogalactopyranoside (IPTG) used to induce CHMO$_{Acineto}$ expression was added to a final concentration of 0.2 mM and the incubation was continued for additional 16 h at 20 °C, 200rpm until the OD_{600} reached between 2.7 and 3.0. Then the cells were harvested by centrifugation (30 min, 5000 rpm, 4°C) and were flushed by 50 mM PBS (pH 7.4) three times. The water covering the cell pellets were removed by nitrogen flow. The weighing wet cells were resuspended in the fresh 50 mM PBS (pH 7.4) to obtain a final concentration of 0.1g.mL^{-1}.

In the whole cell screening protocol, the reaction system contained 1 mL cell culture (0.1g.mL^{-1}) and 2 μL of a stock solution of 0.5 M ketones in acetonitrile). The mixture in 10 ml glass tube with a sealed cap was shaken at 200 rpm and 22 °C for desymmetrization, and the reaction time is 32 h. The reaction was stopped and the mixture was extracted with 1 mL ethyl acetate three times. The sample was analyzed by chiral gas chromatographic analyses (GC) (CP-chirasil-DEX CB 25 cm×0.25 cm) to determine the conversion and the enantiomeric excess of the residues and product.

General procedure for scaling-up Baeyer–Villiger oxidation

The weighing wet cells were resuspended in the fresh 1L 50 mM PBS (pH 7.4) to obtain a final concentration of 0.1g·mL^{-1}. To reduce substrate inhibition, batch-fed method was adopted. Equal amounts of total ketones **1a** were added per 8h three times separately with a final concertation 12mM in 1L reaction system. The reaction was stopped by adding sodium chloride. The system was extracted with ethyl acetate (3 x 500 mL), dried over $MgSO_4$ and a sample was collected for the GC analysis. Then the organic layers were concentrated in *vacuo* and the crude reaction products were purified directly by column chromatography on silica gel (petroleum ether/EtOAc = 4/1) to afford **2a** as a white solid.

2. Additional tables and figures

Table S1. List of forward and reverse primers

Primers	Sequence
forward F432A	GGACCGAATGGCCCGGCTACCAACCTGCCG
forward F432C	GGACCGAATGGCCCGTGCACCAACCTGCCG
forward F432D	GGACCGAATGGCCCGGATACCAACCTGCCG
forward F432E	GGACCGAATGGCCCGGAAACCAACCTGCCG
forward F432G	GGACCGAATGGCCCGGGTACCAACCTGCCG
forward F432H	GGACCGAATGGCCCGCATACCAACCTGCCG
forward F432I	GCTTGGACCGAATGGCCCGATTACCAAC
forward F432K	GGACCGAATGGCCCGAAAACCAACCTGCCG
forward F432L	GAATGGCCCGCTTACCAACCTGCCGCCATCA
forward F432M	GGACCGAATGGCCCGATGACCAACCTGCCG
forward F432N	GGACCGAATGGCCCGAATACCAACCTGCCG
forward F432P	GGACCGAATGGCCCGCCGACCAACCTGCCG

forward F432Q	GAATGGCCCGCAGACCAACCTGCCGCCATCA
forward F432R	GGACCGAATGGCCCGCGTACCAACCTGCCG
forward F432S	GGACCGAATGGCCCGAGTACCAACCTGCCG
forward F432T	GGACCGAATGGCCCGACCACCAACCTGCCG
forward F432V	GAATGGCCCGGTAACCAACCTGCCGCCATCA
forward F432W	GAATGGCCCGTGGACCAACCTGCCGCCATCA
forward F432Y	GGACCGAATGGCCCGTATACCAACCTGCCG
forward L435A	GTTTACCAACGCTCCGCCATCAATTG
forward L435C	GTTTACCAACTGTCCGCCATCAATTG
forward L435D	CCCGTTTACCAACGACCCGCCATCAATTG
forward L435E	CCCGTTTACCAACGAGCCGCCATCAATTG
forward L435G	GTTTACCAACGGTCCGCCATCAATTG
forward L435H	GTTTACCAACCATCCGCCATCAATTG
forward L435I	CCCGTTTACCAACATCCCGCCATCAATTG
forward L435K	CCCGTTTACCAACAAACCGCCATCAATTG
forward L435F	GTTTACCAACTTTCCGCCATCAATTG
forward L435M	GTTTACCAACATGCCGCCATCAATTG
forward L435N	CCCGTTTACCAACAACCCGCCATCAATTG
forward L435P	GTTTACCAACCCTCCGCCATCAATTG
forward L435Q	CCCGTTTACCAACCAGCCGCCATCAATTG
forward L435R	CCCGTTTACCAACCGGCCGCCATCAATTG
forward L435S	CCCGTTTACCAACAGCCCGCCATCAATTG
forward L435T	GTTTACCAACACCCCGCCATCAATTG
forward L435V	CCCGTTTACCAACGTGCCGCCATCAATTG
forward L435W	GTTTACCAACTGGCCGCCATCAATTG
forward L435Y	GTTTACCAACTATCCGCCATCAATTG
forward L143A	ACTGCTTTAGGCGCCTTGTCTGCGCCTAAC
forward L143F	ACTGCTTTAGGCTTCTTGTCTGCGCCTAAC
forward F505A	CACGGTTTACGCGTATCTCGGTGG
forward F505L	CACGGTTTACTATCTCGGTGG
Silent reverse primer	GCGGCCGCTCTGGATCCATGC

Table S2. WT CHMO$_{Acineto}$ as the catalysts in the desymmetrization of prochiral cyclohexanones 1[a]

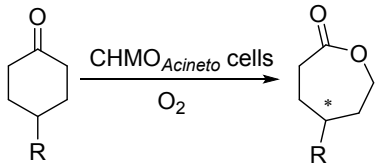

1 **(-)-2** or **(+)-2**

a R = Ph
b R = 3-MeC_6H_4
c R = 4-MeC_6H_4
d R = 3-FC_6H_4
e R = 4-FC_6H_4
f R = 4-$CH_3OC_6H_4$
g R = 4-ClC_6H_4
h R = *n*-Pentyl
i R = ^{n}Pr
j R = Et
k R = Me

Entry	Substrate	Product	Conv. (%)[b]	ee$_p$(%)[c]
1	**1a**	**2a**	99	98(-)
2	**1b**	**2b**	99	76(-)
3	**1c**	**2c**	99	52(-)
4	**1d**	**2d**	99	75(-)
5	**1e**	**2e**	99	90(-)
6	**1f**	**2f**	99	53(-)
7	**1g**	**2g**	99	54(-)
8	**1h**	**2h**	99	33(+)
9	**1i**	**2i**	99	94(*S*)(-)[d]
10	**1j**	**2j**	99	98(*S*)(-)[d]
11	**1k**	**2k**	99	99(*S*)(-)[d]

[a] The whole cell experiments are described in Experiment section. [b, c] Determined by chiral GC. [d] The absolute configuration was confirmed by comparison with the literature[12].

Table S3. Potential CHMO$_{Acineto}$ mutants as catalysts in the desymmetrization of prochiral cyclohexanones 1a[a]

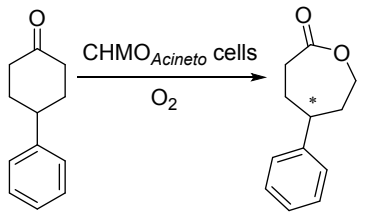

1a **(-)-2a** or **(+)-2a**

Entry	Enzyme	Conv.(%)[b]	ee$_p$(%)[c]
1	L143A	99	98(-)
2	L143F	99	98(-)
3	F432A	85	95(-)
4	L435F	<3	-
5	F505A	99	96(-)
6	F505L	99	96(-)

[a] The whole cell experiments are described in Experiment section. [b, c] Determined by chiral GC.

Table S4. F432X mutants as catalysts in the desymmetrization of prochiral-cyclohexanones 1a[a]

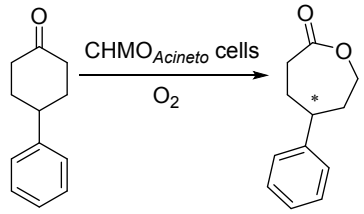

1a **(-)-2a** or **(+)-2a**

Entry	Enzyme	Conv.(%)[b]	ee$_p$(%)[c]
1	F432C	60	30(-)
2	F432D	23	90(-)
3	F432E	52	92(-)
4	F432G	75	99(-)
5	F432H	67	96(-)
6	F432K	89	96(-)
7	F432M	99	89(-)
8	F432N	98	98(-)
9	F432P	99	98(-)
10	F432Q	99	99(-)
11	F432R	<3	-
12	F432S	99	98(-)
13	F432T	99	98(-)
14	F432V	99	85(-)
15	F432W	<3	-
16	F432Y	<3	-

[a] The whole cell experiments are described in Experiment section. [b, c] Determined by chiral GC.

Table S5. L435X mutants as catalysts in the desymmetrization of prochiral-cyclohexanones 1a[a]

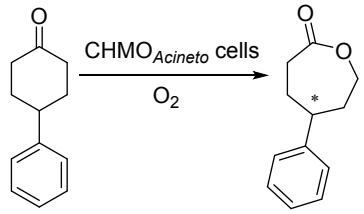

1a **(-)-2a** or **(+)-2a**

Entry	Enzyme	Conv.(%)[b]	ee$_p$(%)[c]
1	L435C	89	95(-)
2	L435D	<3	-
3	L435E	9	99(-)
4	L435H	90	99(-)
5	L435I	99	98(-)
6	L435K	<3	-
7	L435M	99	55(-)
8	L435N	<3	-
9	L435P	<3	-
10	L435Q	<3	-
11	L435R	<3	-
12	L435S	99	1(-)
13	L435T	46	75(-)
14	L435V	99	99(-)
15	L435W	<3	-
16	L435Y	<3	-

[a] The whole cell experiments are described in Experiment section. [b, c] Determined by chiral GC.

Table S6. The amplified reaction of substrate 1a by the WT and the best mutants[a]

Entry	Variants	Conversion/% [b]	*ee*/% [b]	Yield/%[c]
1	WT	95	98 (-)	78
2	F432L	92	95 (+)	72
3	L435A	70	98 (+)	51

[a] The experiments are described in Experiment section. [b] Determined by chiral GC. [c] Isolated yield calculated by isolation of products using column chromatography.

Table S7. WT CHMO$_{Acineto}$ and mutants as catalysts in the BV oxidation of 2-methyl cyclohexanone (3) and 3-methyl cyclohexanone (6)[a]

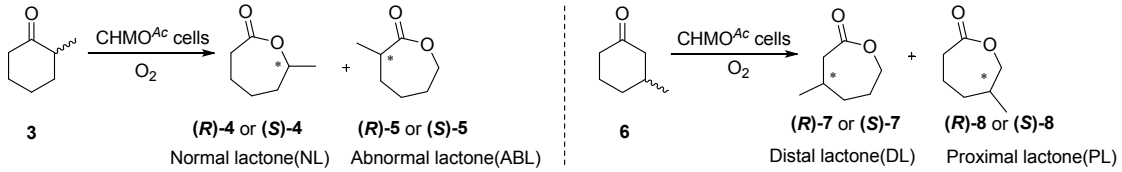

Entry	Substrate	Enzymes	Conv. (%)	Products (NL or DL)			Products (ABL or PL)			Regioisomeric ratio
				Lactone	ee$_p$(%)[a] (config.[b])	*E*-value	Lactone	ee$_p$(%)[a] (config.[b])	*E*-value	
1	**3**	WT	30	**4**	64 (*S*)	5.9	**5**	ND[c]	ND	NL:ABL>99:1
2	**3**	F432L	28	**4**	68 (*S*)	6.8	**5**	ND	ND	NL:ABL>99:1
3	**3**	L435A	32	**4**	69 (*S*)	7.4	**5**	ND	ND	NL:ABL>99:1
4	**6**	WT	32	**7**	99 (*S*)	ND	**8**	97 (*R*)	ND	DL:PL=51:49
5	**6**	F432L	30	**7**	99 (*S*)	ND	**8**	97 (*R*)	ND	DL:PL=55:45
6	**6**	L435A	34	**7**	99 (*S*)	ND	**8**	97 (*R*)	ND	DL:PL=51:49

[a] Determined by chiral GC. [b] The absolute configurations were confirmed by comparison with literature values. [13-14] [c] ND: not determined.

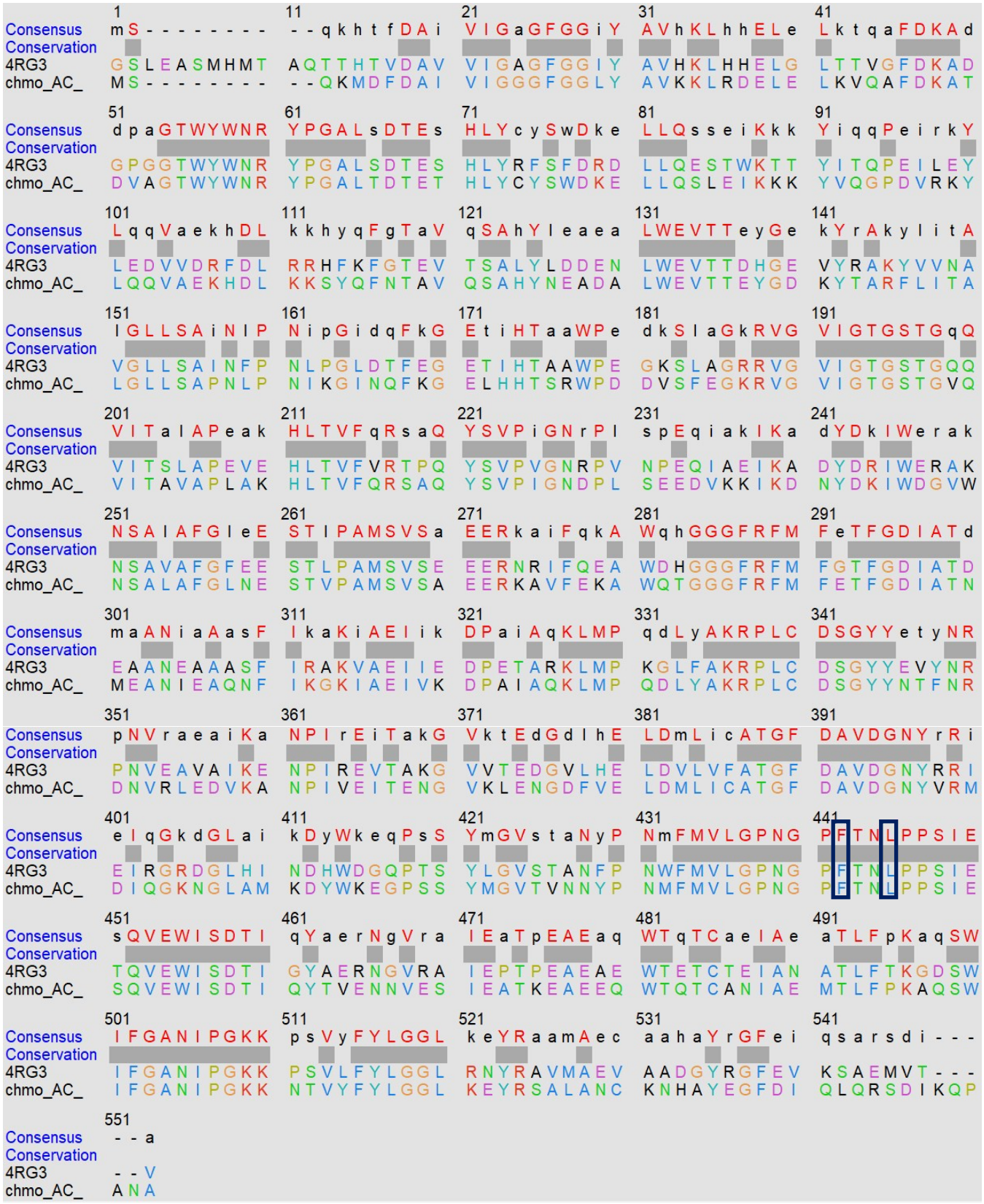

Figure S1. The sequence alignment of CHMO from *Acinetobacter* sp. NCIMB 9871 and CHMO*Rhodococcus* sp. strain HI-31 (PDB code: 4RG3). The key residues Phe432 and Leu435 (numbered in $CHMO_{Acineto}$) are highlighted by rectangle.

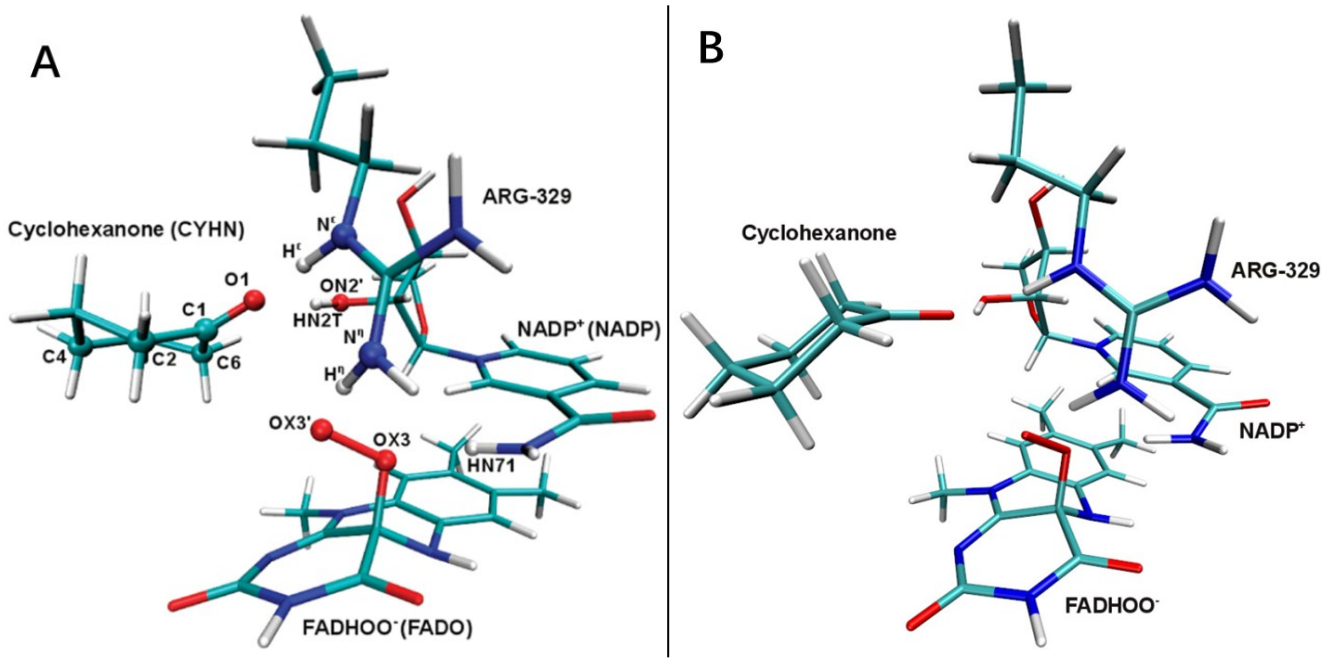

Figure S2. A) Enzyme-reactant complex with the cyclohexanone relative to the preferred orientation. B) Enzyme-reactant complex with the cyclohexanone relative to the unfavorable orientation, being flipped around its main axis by 180^{o}. Note: The pictures stem from Reference 1a.

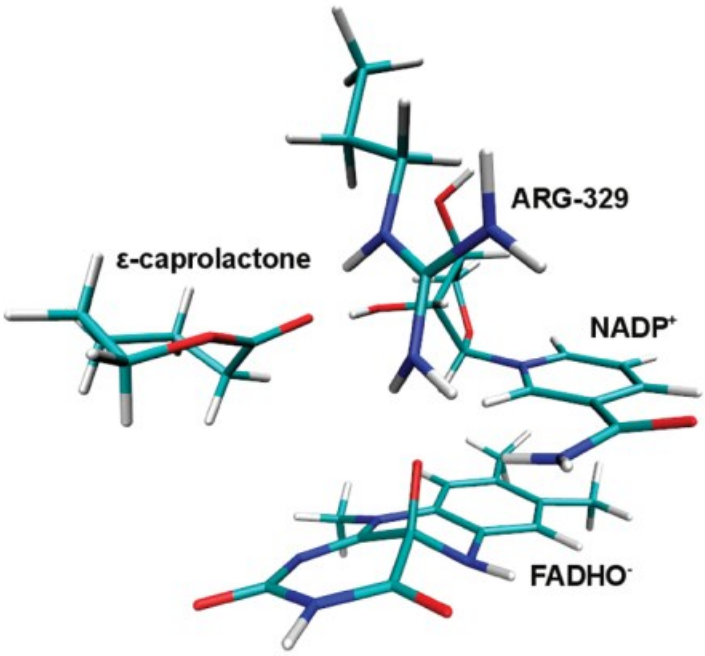

Figure S3. Enzyme-product complex with the well-defined product. Note: The pictures stem from Reference 1a.

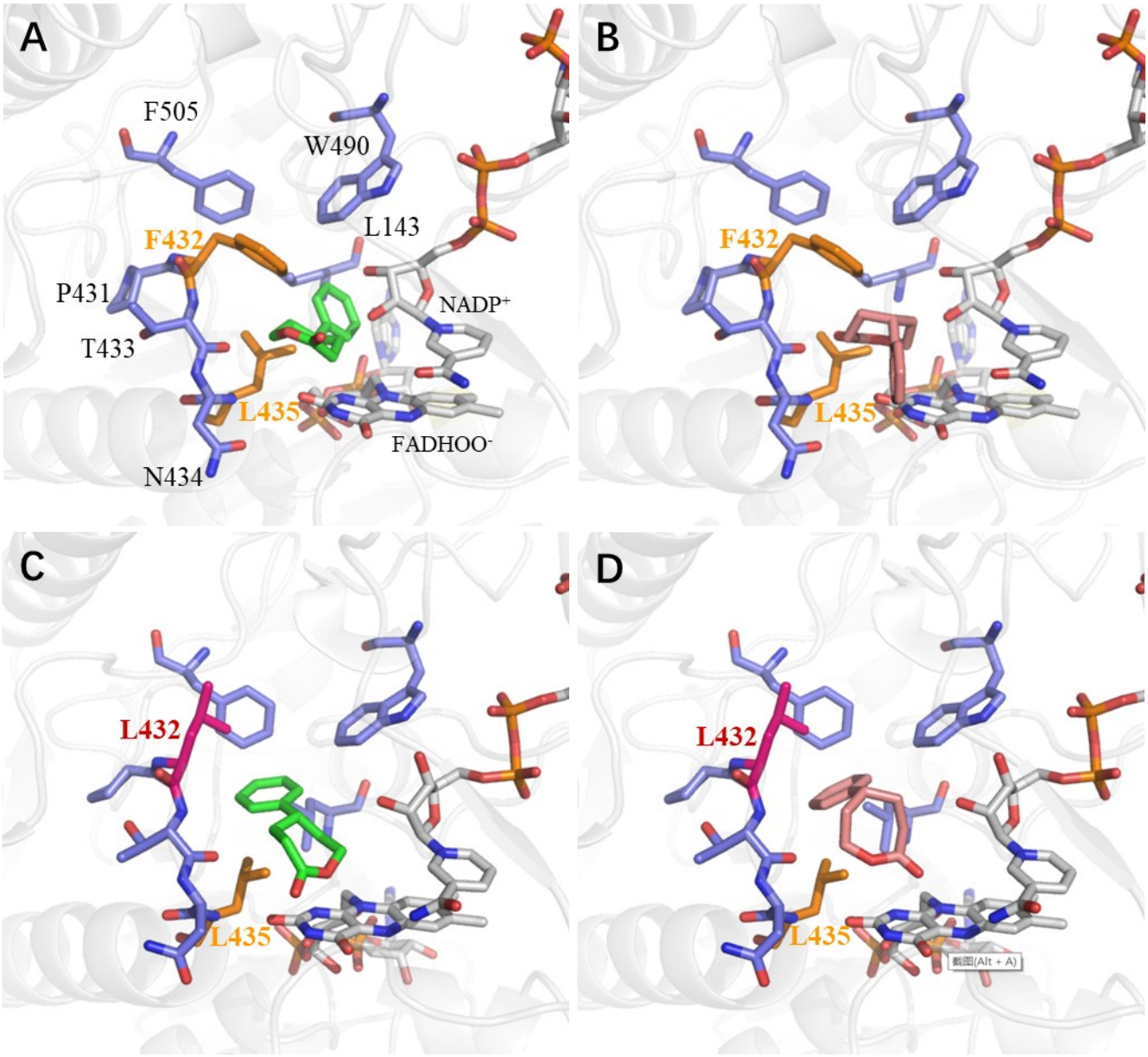
A
F505
W490
L143
F432
P431
NADP+
T433
L435
FADHOO-
N434
B
F432
L435
C
L432
L435
D
L432
L435

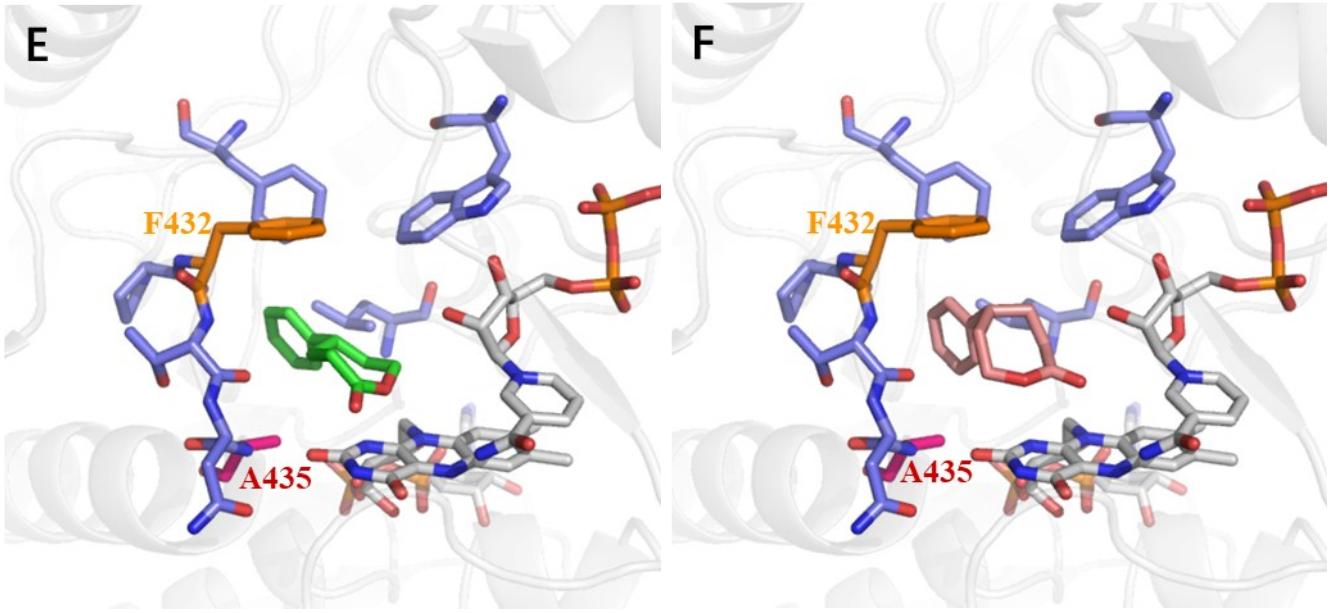

Figure S4. A) (*S*)-**2a** (green) docked in the active site of WT. B) (*R*)-**2a** (salmon) docked in the active site of WT. C) (*S*)-**2a** (green) docked in the active site of the mutant F432L. D) (*R*)-**2a** (salmon) docked in the active site of the mutant F432L. E) (*S*)-**2a** (green) docked in the active site of the mutant L435A. F) (*R*)-**2a** (salmon) docked in the active site of the mutant L435A.

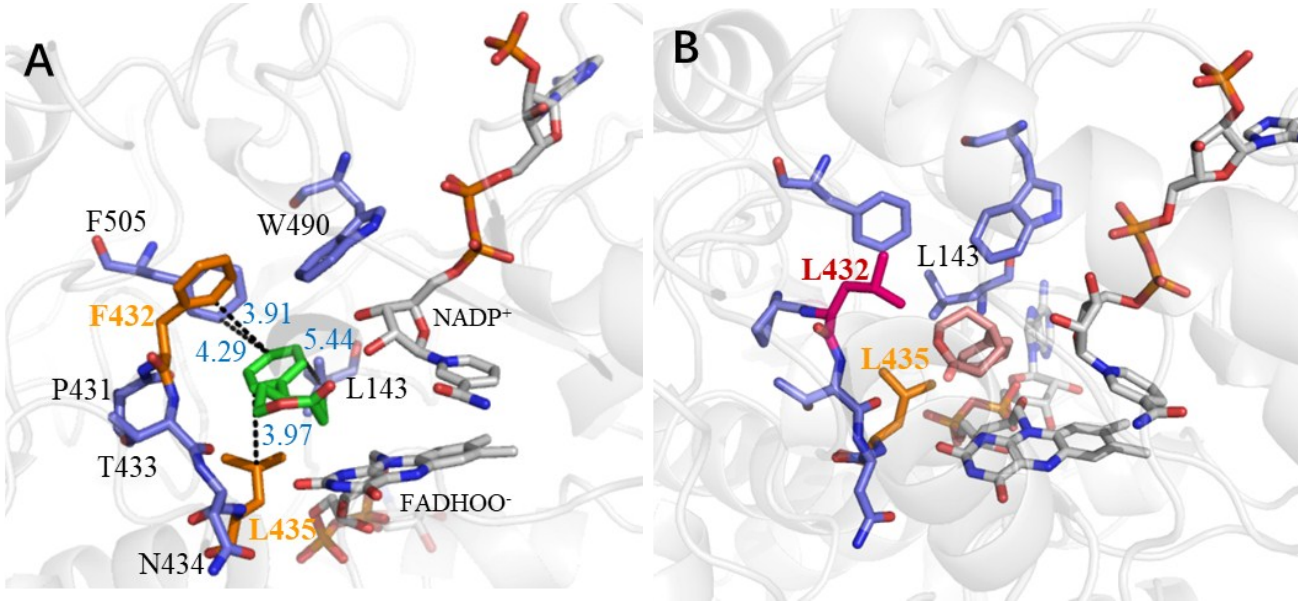

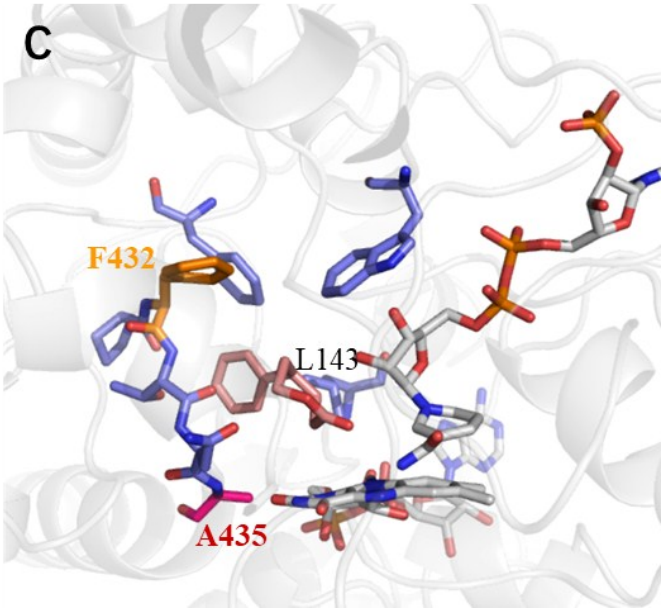

Figure S5. MD optimized structures are shown with sticks. A) WT $CHMO_{homo}$ in complex with (*S*)-**2a**, B) $CHMO_{homo}$ mutant F432L in complex with (*R*)-**2a**. C) $CHMO_{homo}$ mutant L435A in complex with (*R*)-**2a**. The unit of distances is shown in Å.

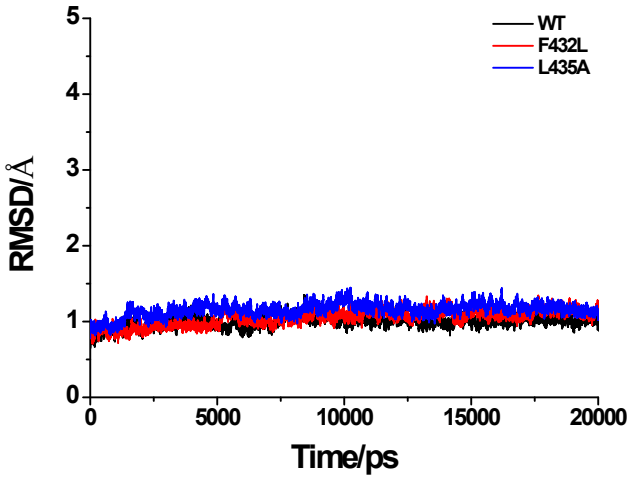

Figure S6. RMSD of the alpha-carbon atoms in MD dynamics for the WT with (*S*)-**2a** (black); the mutant F432L with (*R*)-**2a** (red); the mutant L435A with (*R*)-**2a** (blue).

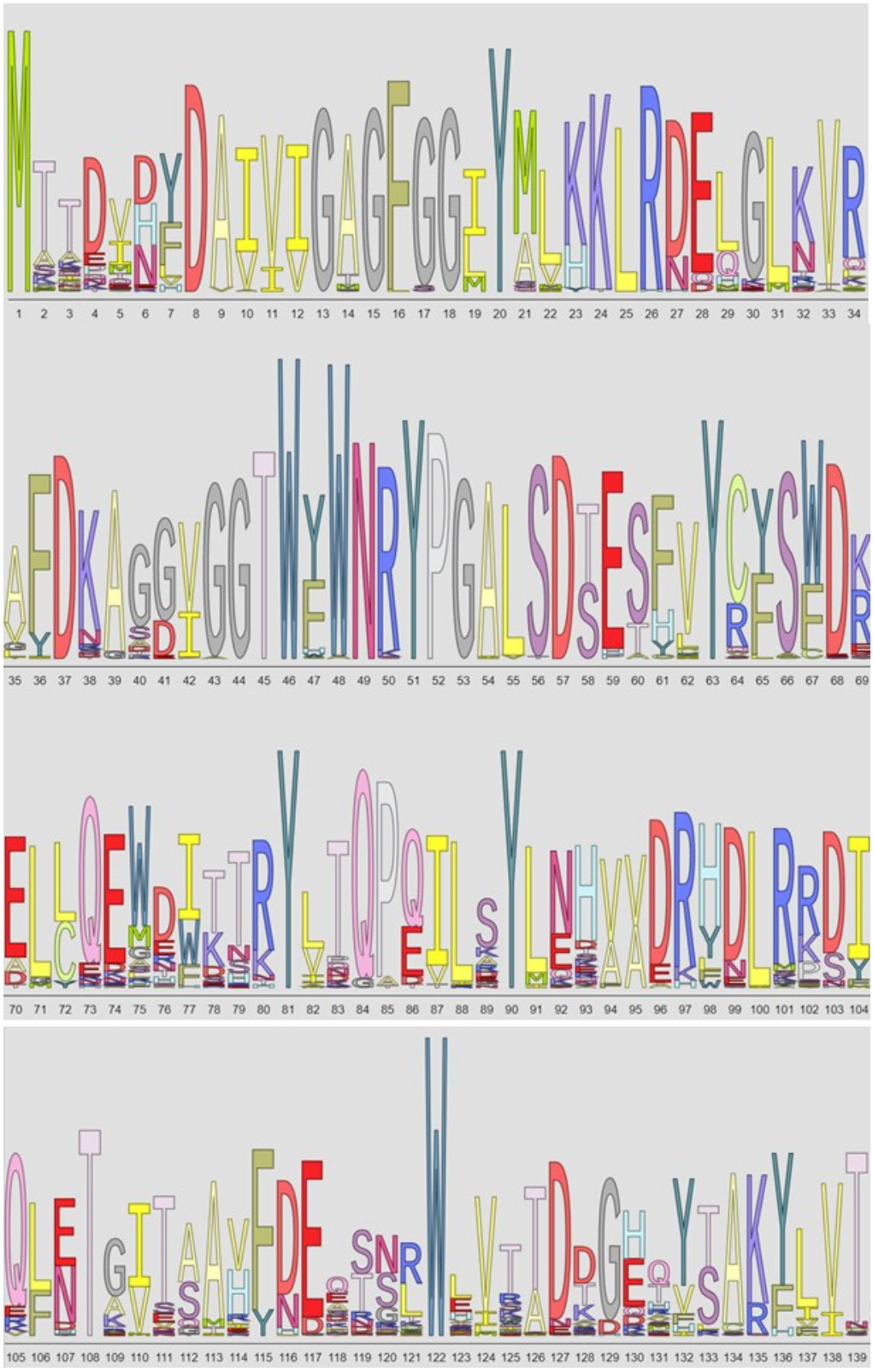
1 2 3 4 5 6 7 8 9 10 11 12 13 14 15 16 17 18 19 20 21 22 23 24 25 26 27 28 29 30 31 32 33 34
35 36 37 38 39 40 41 42 43 44 45 46 47 48 49 50 51 52 53 54 55 56 57 58 59 60 61 62 63 64 65 66 67 68 69
70 71 72 73 74 75 76 77 78 79 80 81 82 83 84 85 86 87 88 89 90 91 92 93 94 95 96 97 98 99 100 101 102 103 104
105 106 107 108 109 110 111 112 113 114 115 116 117 118 119 120 121 122 123 124 125 126 127 128 129 130 131 132 133 134 135 136 137 138 139

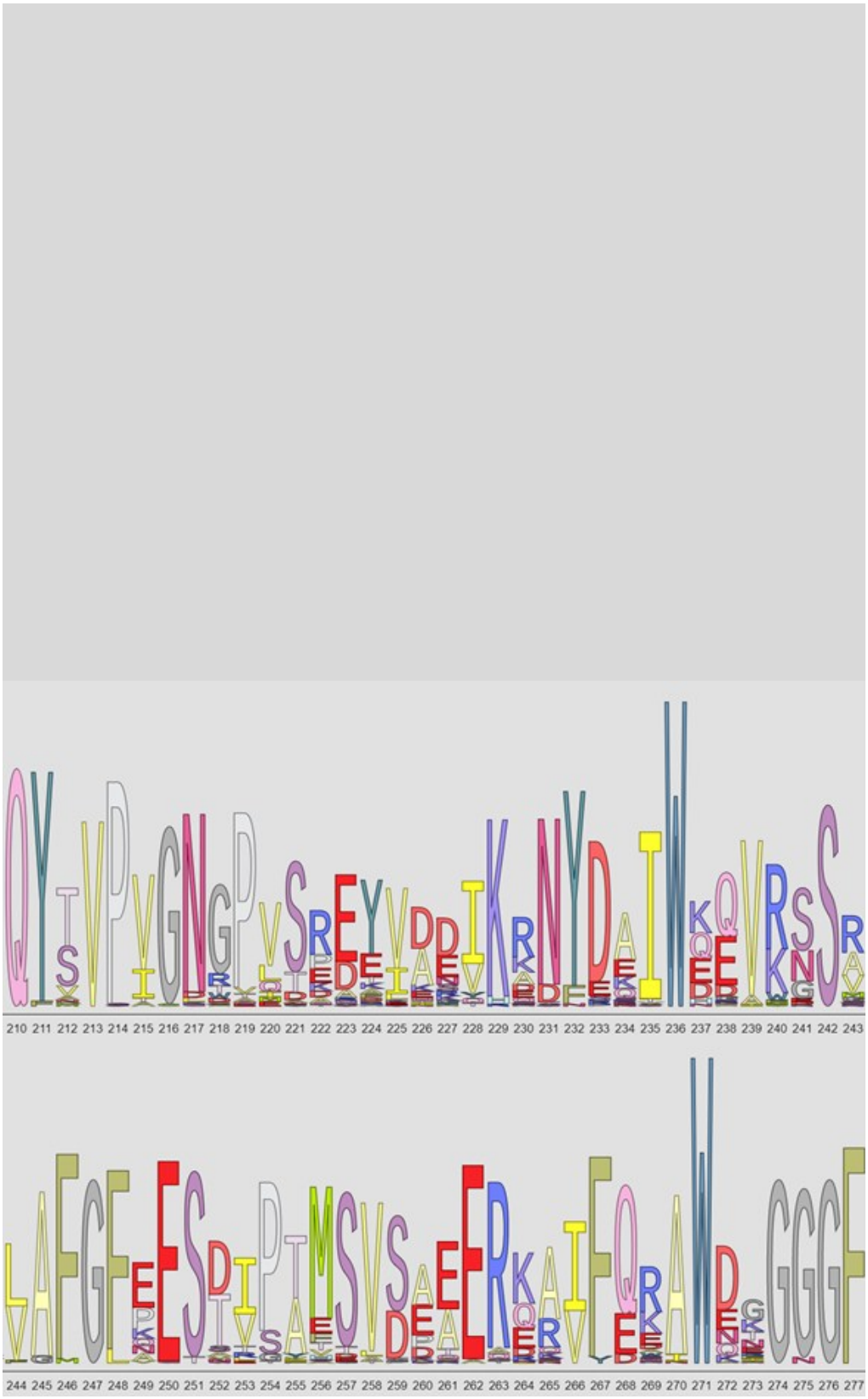
210 211 212 213 214 215 216 217 218 219 220 221 222 223 224 225 226 227 228 229 230 231 232 233 234 235 236 237 238 239 240 241 242 243
244 245 246 247 248 249 250 251 252 253 254 255 256 257 258 259 260 261 262 263 264 265 266 267 268 269 270 271 272 273 274 275 276 277

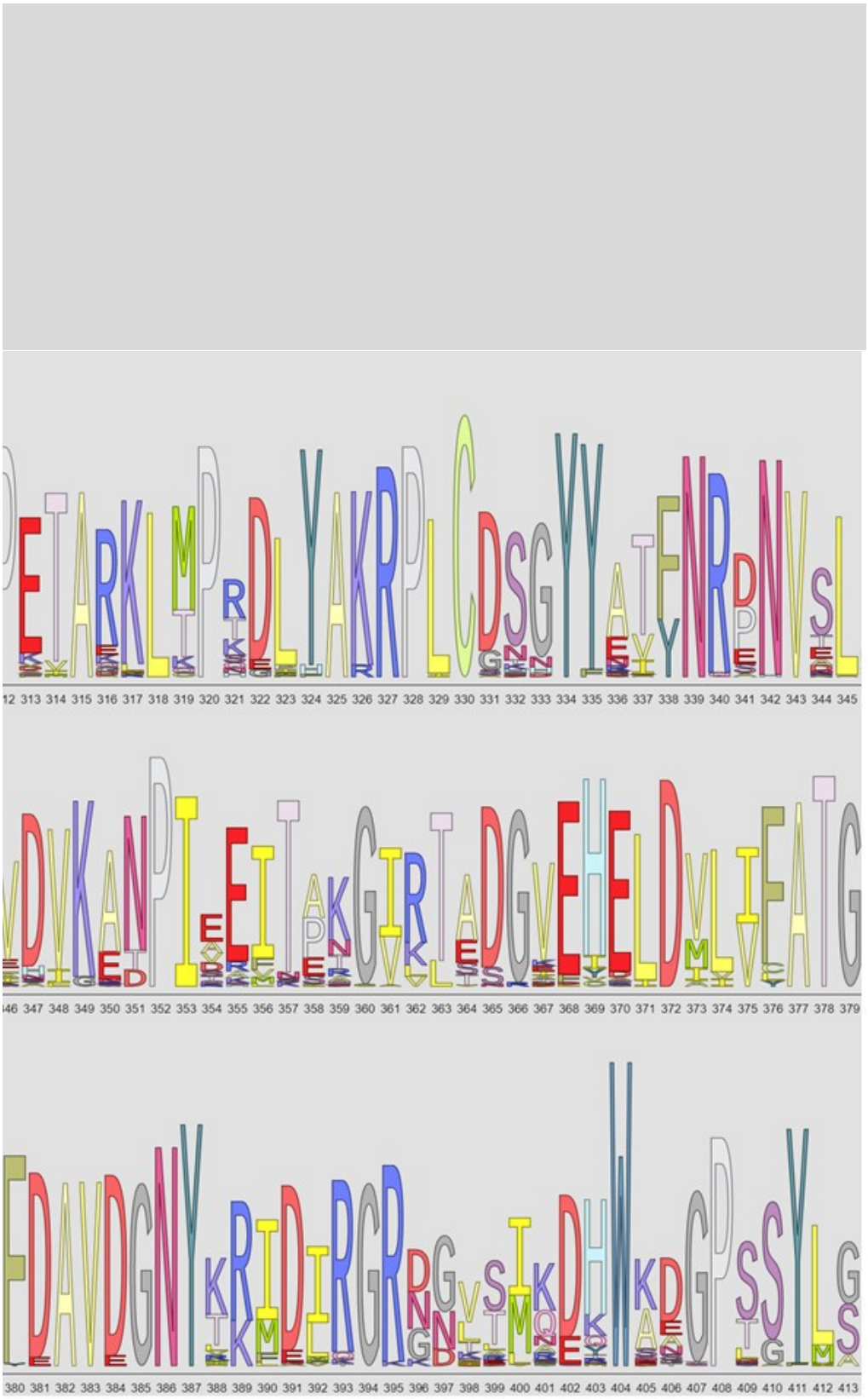
12 313 314 315 316 317 318 319 320 321 322 323 324 325 326 327 328 329 330 331 332 333 334 335 336 337 338 339 340 341 342 343 344 345
346 347 348 349 350 351 352 353 354 355 356 357 358 359 360 361 362 363 364 365 366 367 368 369 370 371 372 373 374 375 376 377 378 379
380 381 382 383 384 385 386 387 388 389 390 391 392 393 394 395 396 397 398 399 400 401 402 403 404 405 406 407 408 409 410 411 412 413

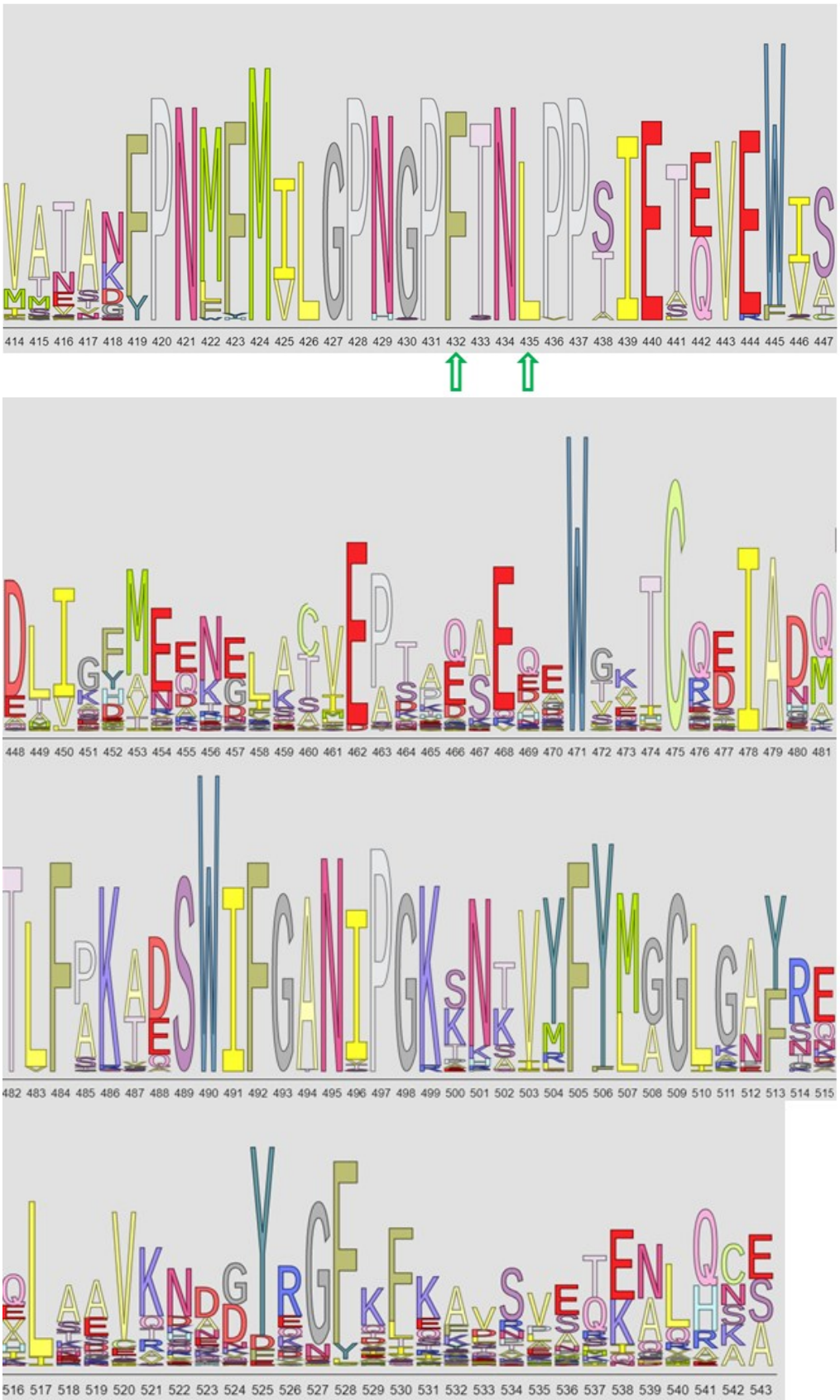

Figure S7. Sequence comparison of 94 homologous BVMO sequences identified using CHMO from *Acinetobacter sp.* NCIMB 9871 as the reference.

3. NMR data of obtained lactones.

5-phenyloxepan-2-one (2a): ^{1}H NMR (400 MHz, $CDCl_3$): δ = 7.25 (t, *J* = 7.2 Hz, 2H), 7.14 (d, *J* = 8.0 Hz, 1H), 7.08 (d, *J* = 7.2 Hz, 2H), 4.27–4.16 (m, 2H), 2.77–2.62 (m, 3H), 2.03–1.83 (m, 3H), 1.83–1.64 (m, 1H). ^{13}C NMR (100 MHz, CDCl3) δ = 175.91, 145.09, 128.78, 126.85, 126.68, 68.27, 47.07, 36.71, 33.69, 30.32 ppm.

5-(*m*-tolyl)oxepan-2-one (2b): ^{1}H NMR (400 MHz, $CDCl_3$): δ = 7.21 (t, *J* = 7.6 Hz, 1H), 7.06 (d, *J* = 7.6 Hz, 1H), 6.99–6.97 (m, 2H), 4.42–4.28 (m, 2H), 2.85–2.71 (m, 3H), 2.34 (s, 3H), 2.16–1.94 (m, 3H), 1.90–1.77 (m, 1H). ^{13}C NMR (100 MHz, $CDCl_3$) δ = 175.79, 144.96, 138.41, 128.67, 127.61, 127.43, 123.63, 68.32, 47.24, 36.76, 33.74, 30.35, 21.47 ppm

5-(*p*-tolyl)oxepan-2-one (2c): ^{1}H NMR (400 MHz, $CDCl_3$): δ = 7.15 (d, *J* = 8.0 Hz, 2H), 7.08 (d, *J* = 8.0 Hz, 2H), 4.41–4.28 (m, 2H), 2.85–2.71 (m, 3H), 2.33 (s, 3H), 2.19–1.96 (m, 3H), 1.87–1.77 (m, 1H). ^{13}C NMR (100 MHz, $CDCl_3$) δ = 175.81, 142.04, 136.48, 129.43, 126.49, 68.31, 46.84, 36.83, 33.72, 30.44, 21.01 ppm.

5-(3-fluorophenyl)oxepan-2-one (2d): ^{1}H NMR (400 MHz, $CDCl_3$): δ = 7.31–7.28 (m, 1H), 6.98–6.87 (m, 3H), 4.43–4.28 (m, 2H), 2.87–2.76 (m, 3H), 2.20–1.93 (m, 3H), 1.89–1.74 (m, 1H). ^{13}C NMR (100 MHz, $CDCl_3$) δ = 175.42, 164.22, 161.78, 147.45, 147.38, 130.35, 130.27, 122.26, 122.24, 113.88, 113.76, 113.67, 113.54, 68.01, 46.92, 36.59, 33.57, 30.15 ppm.

5-(4-fluorophenyl)oxepan-2-one (2e): ^{1}H NMR (400 MHz, $CDCl_3$): δ = 7.15 (dd, *J* = 8.8, 5.6 Hz, 2H), 7.03 (t, *J* = 8.4 Hz, 2H), 4.38–4.27 (m, 3H), 2.88–2.72 (m, 3H), 2.16–1.95 (m, 3H), 1.86–1.76 (m, 1H). ^{13}C NMR (100 MHz, $CDCl_3$) δ = 175.53, 162.85, 160.41, 140.70, 140.67, 128.07, 127.99, 115.67, 115.46, 68.11, 46.51, 36.92, 33.62, 30.50 ppm.

5-(4-methoxyphenyl)oxepan-2-one (2f): ^{1}H NMR (400 MHz, $CDCl_3$): δ = 7.11 (d, *J* = 8.4 Hz, 2H), 6.87 (d, *J* = 8.4 Hz, 2H), 4.41–4.27 (m, 2H), 3.79 (s, 3H), 2.83–2.71 (m, 3H), 2.13–1.92 (m, 3H), 1.87–1.74 (m, 1H). ^{13}C NMR (100 MHz, $CDCl_3$) δ = 175.81, 158.37, 137.20, 127.54, 114.10, 68.30, 55.30, 46.40, 36.97, 33.69, 30.59 ppm.

5-(4-chlorophenyl)oxepan-2-one (2g): ^{1}H NMR (400 MHz, $CDCl_3$): δ = 7.30 (d, *J* = 8.4 Hz, 1H), 7.13 (d, *J* = 8.4 Hz, 1H), 4.42-4.28 (m, 2H), 2.88–2.72 (m, 3H), 2.15–1.94 (m, 3H), 1.85–1.75 (m, 1H). ^{13}C NMR (100 MHz, $CDCl_3$) δ = 175.44, 143.35, 132.58, 128.93, 127.98, 68.05, 46.63, 36.70, 33.60, 30.28 ppm.

5-pentyloxepan-2-one (2h): ^{1}H NMR (400 MHz, $CDCl_3$): δ = 4.30–4.25 (m, 1H), 4.15 (dd, *J* = 12.8, 10.4 Hz, 1H), 2.69–2.71 (m, 1H), 2.60–2.54 (m, 1H), 1.98–1.87 (m, 2H), 1.63-1.54 (m, 1H), 1.50–1.40 (m, 1H), 1.33-1.15 (m, 9H), 0.86 (t, *J* = 6.4 Hz, 3H). ^{13}C NMR (100 MHz, $CDCl_3$): δ = 176.42, 68.29, 40.22, 36.41, 35.34, 33.20, 31.91, 28.89, 26.45, 22.64, 14.10 ppm.

5-propyloxepan-2-one (2i): ^{1}H NMR (400 MHz, $CDCl_3$): δ = 4.29–4.24 (m, 1H), 4.15 (dd, *J* = 12.4, 10.0 Hz, 1H), 2.71–2.65 (m, 1H), 2.64–2.57(m, 1H), 2.01–1.89 (m, 2H), 1.67-1.59 (m, 1H), 1.52–1.43(m, 1H), 1.37-1.23(m, 5H), 0.90 (t, *J* = 7.2 Hz, 3H). ^{13}C NMR (100 MHz, $CDCl_3$): δ = 176.28, 68.24, 39.90, 38.66, 35.32, 33.20, 28.87, 19.86, 14.16 ppm.

5-ethyloxepan-2-one (2j): ^{1}H NMR (400 MHz, $CDCl_3$): δ = 4.30–4.25 (m, 1H), 4.15 (dd, *J* = 12.8, 10.0 Hz, 1H), 2.68–2.62 (m, 1H), 2.61–2.54 (m, 1H), 2.00–1.89 (m, 2H), 1.50–1.42 (m, 2H), 1.32–1.22 (m, 3H), 0.88 (t, *J* = 7.2 Hz, 3H). ^{13}C NMR (100 MHz, $CDCl_3$): δ = 176.31, 68.25, 41.86, 34.93, 33.17, 29.14, 28.50, 11.31 ppm.

5-methyloxepan-2-one (2k): ^{1}H NMR (400 MHz, $CDCl_3$): δ = 4.26 (dd, *J* =11.6, 5.6 Hz, 1H), 4.17–4.12 (m, 1H), 2.66–2.54 (m, 2H), 1.97–1.78 (m, 2H), 1.78–1.67 (m, 1H), 1.46 (dt, *J* = 15.2, 10.8 Hz, 1H), 1.35–1.24 (m, 1H), 0.97 (d, *J* = 6.4 Hz, 3H). ^{13}C NMR (100 MHz, $CDCl_3$): δ = 176.17, 68.14, 37.22, 35.27, 33.22, 30.76, 22.16 ppm.

4. Chiral GC data of enantiopure lactones.

Note: The peaks of WT are shown in black, and the peaks of mutants are shown in pink.

5-phenyloxepan-2-one (2a)

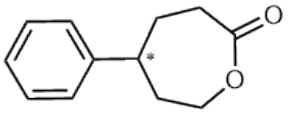

110°C, 2°C/min 200°C, 10 min, t_r(-) = 39.001 min, t_r(+) = 39.461 min.
(-)-enantiomer: 98% *ee*, $[\alpha]_D^{20}$ = -57.0 (c 1.03, $CHCl_3$);
(+)-enantiomer: 99% *ee*, $[\alpha]_D^{20}$ = +58.6 (c 1.18, $CHCl_3$).

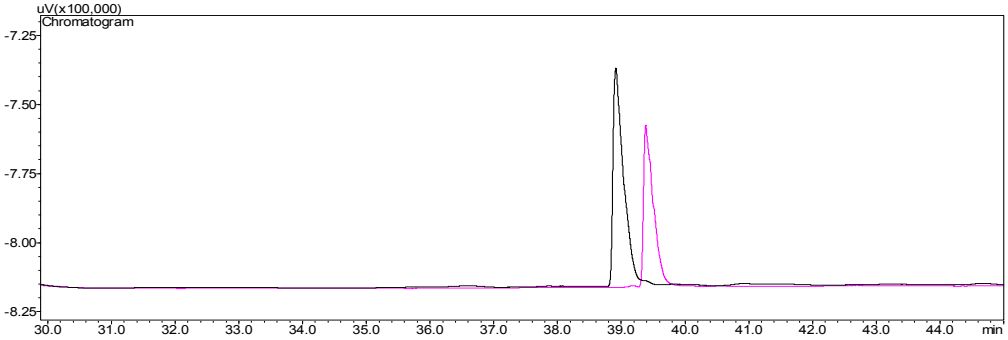

5-(*m*-tolyl)oxepan-2-one (2b)

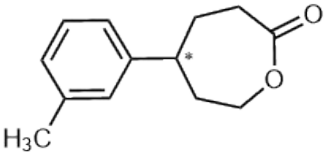

110°C, 2°C/min 200°C, 10 min, t_r(-) = 42.088 min, t_r(+) = 42.335 min.
(-)-enantiomer: 76% *ee*;
(+)-enantiomer: 95% *ee*, $[\alpha]_D^{20}$ = +44.6 (c 0.98, $CHCl_3$).

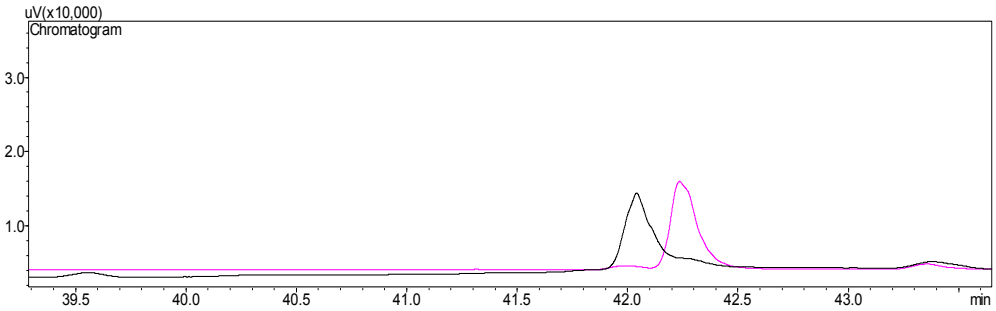

5-(*p*-tolyl)oxepan-2-one (2c)

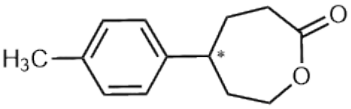

110°C, 2°C/min 200°C, 10 min, t_r(-) = 42.926 min, t_r(+) = 43.336 min.
(-)-enantiomer: 52% *ee*;
(+)-enantiomer: 98% *ee*, $[\alpha]_D^{20}$ = +54.5 (c 0.78, $CHCl_3$).

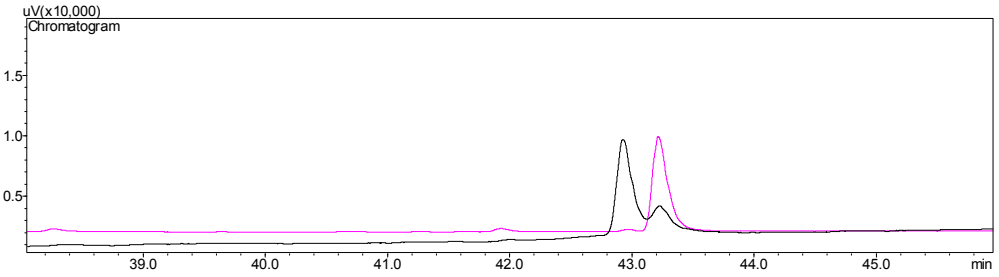

5-(3-fluorophenyl)oxepan-2-one (2d)

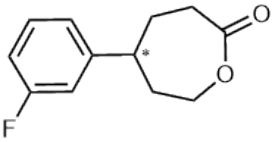

110°C, 2°C/min 200°C, 10 min, t_r(-) = 40.566 min, t_r(+) = 40.915 min.
(-)-enantiomer: 75% *ee*;

(+)-enantiomer: 98% *ee*, $[\alpha]_D^{20}$ = +52.9 (c 0.86, $CHCl_3$).

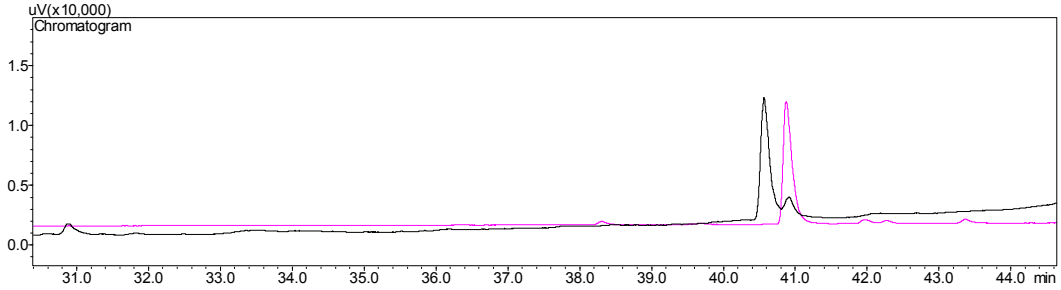

5-(4-fluorophenyl)oxepan-2-one (2e) 110°C, 2°C/min 200°C, 10 min, t_r(-) = 41.255 min, t_r(+) = 41.686 min.

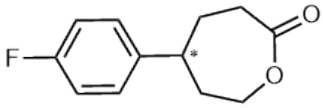

(-)-enantiomer: 90% *ee*;
(+)-enantiomer: 99% *ee*, $[\alpha]_D^{20}$ = +58.7 (c 0.99, $CHCl_3$).

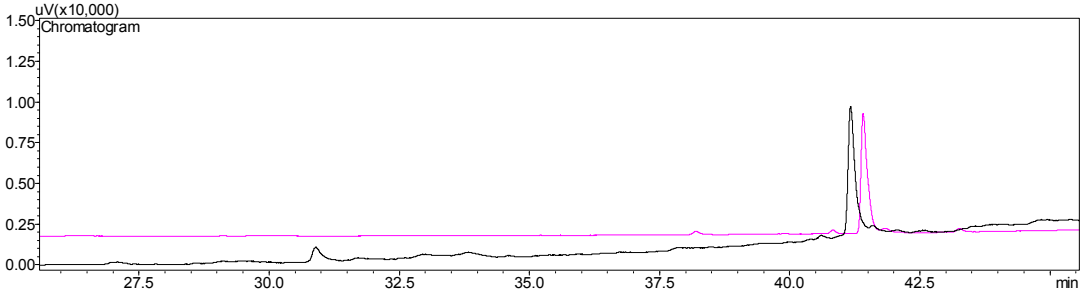

5-(4-methoxyphenyl)oxepan-2-one (2f) 110°C, 2°C/min 200°C, 10 min, t_r(-) = 51.850 min, t_r(+) = 52.235 min.

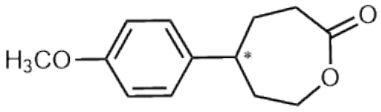

(-)-enantiomer: 53% *ee*;
(+)-enantiomer: 98% *ee*, $[\alpha]_D^{20}$ = +56.3 (c 0.77, $CHCl_3$).

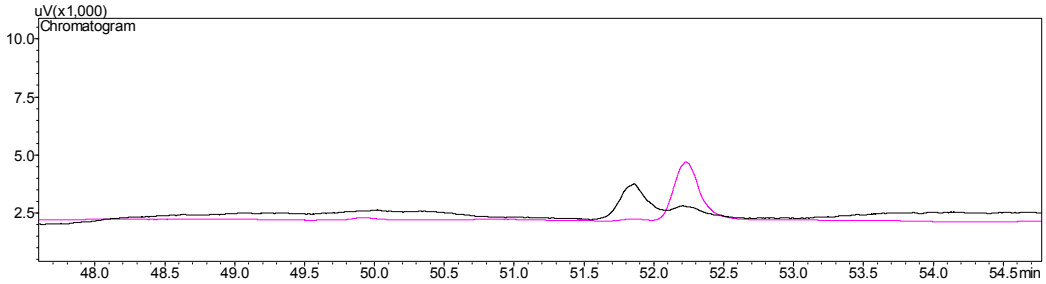

5-(4-chlorophenyl)oxepan-2-one (2g) 110°C, 2°C/min 200°C, 10 min, t_r(-) = 50.718 min, t_r(+) = 51.186 min.

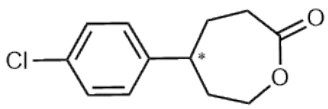

(-)-enantiomer: 54% *ee*;

(+)-enantiomer: 97% *ee*, $[\alpha]_D^{20}$ = +49.5 (c 1.08, $CHCl_3$).

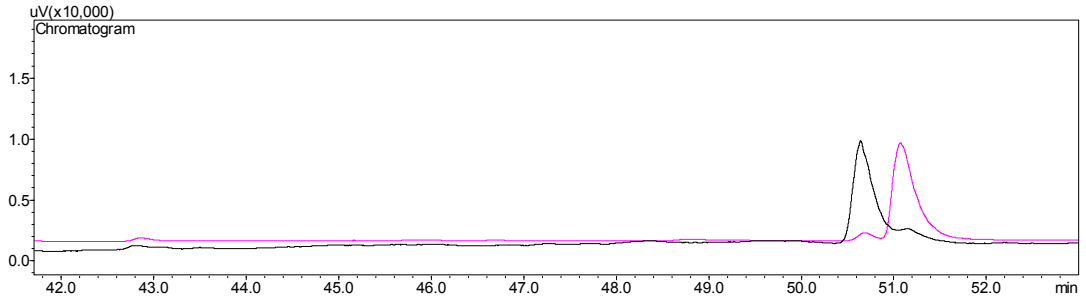

5-pentyloxepan-2-one (2h) 116°C, 2°C/min 180°C, t_r (-) = 28.28 min, t_r (+) = 28.518 min.
(+)-enantiomer: 85% *ee*, $[\alpha]_D^{20}$ = +26.3 (c 0.79, $CHCl_3$).

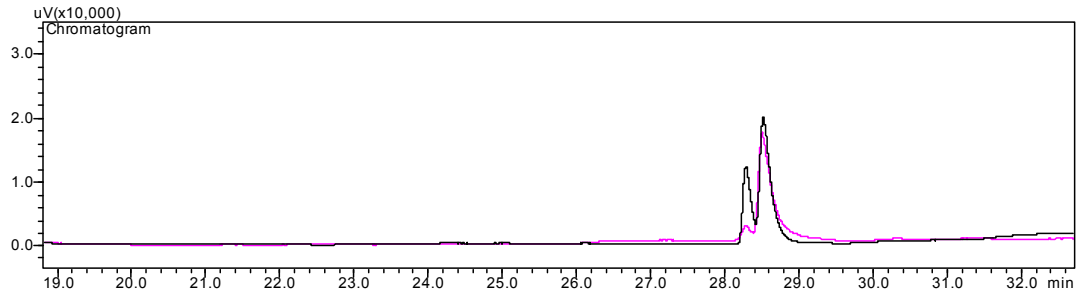

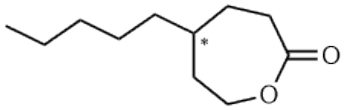

5-propyloxepan-2-one (2i) 110°C, 2°C/min, 170°C, t_r (*S*) = 19.860 min, t_r (*R*) = 20.217 min.

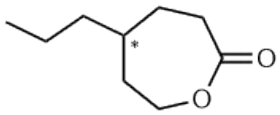

(*S*)-enantiomer: 94% *ee*, $[\alpha]_D^{20}$ = -44.0 (c 1.23, $CHCl_3$);
(*R*)-enantiomer: 70% *ee*.

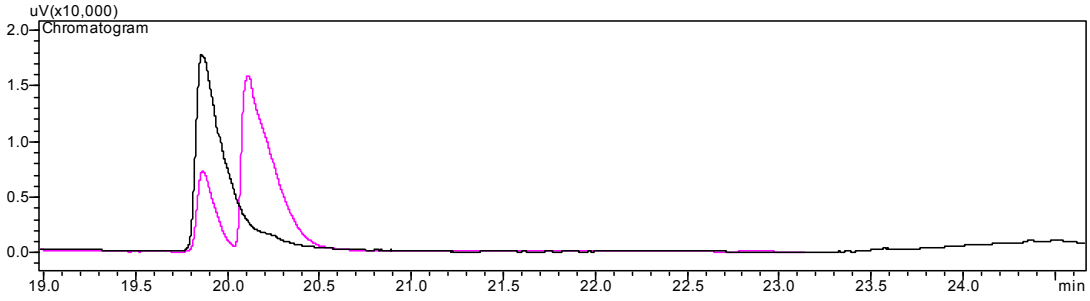

5-ethyloxepan-2-one (2j) 110°C, 2°C/min, 170°C, t_r (*S*) = 14.835 min, t_r (*R*) = 15.146 min.
(*S*)-enantiomer: 98% *ee*, $[\alpha]_D^{20}$ = -47.4 (c 0.98, $CHCl_3$).

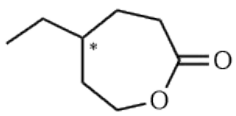

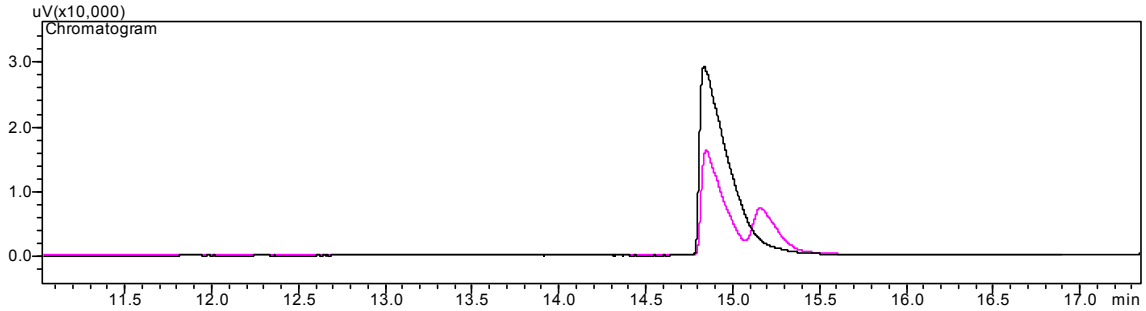

5-methyloxepan-2-one (2k)

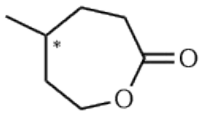

100°C, 2°C/min, 170°C, t_r (*S*) = 14.383 min, t_r (*R*) = 14.747 min.
(*S*)-enantiomer: 99% *ee*, $[\alpha]_D^{20}$ = -50.3 (c 0.99, $CHCl_3$).

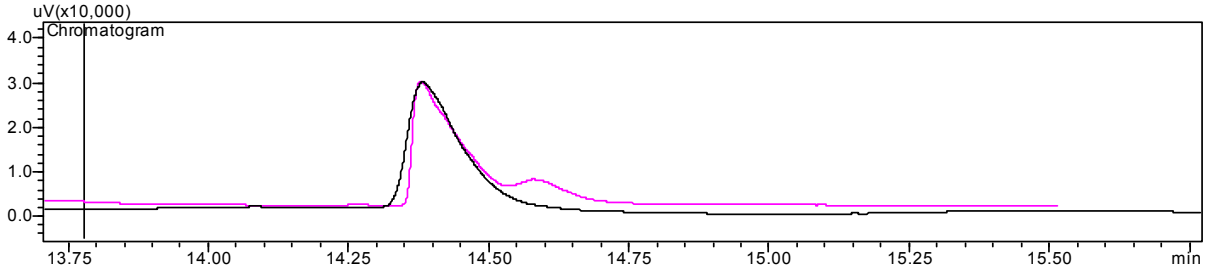

7-methyloxepan-2-one (4)

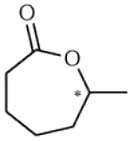

60°C, 2°C/min 150 °C, t_r (*S*) = 24.338 min, t_r (*R*) = 25.633 min.

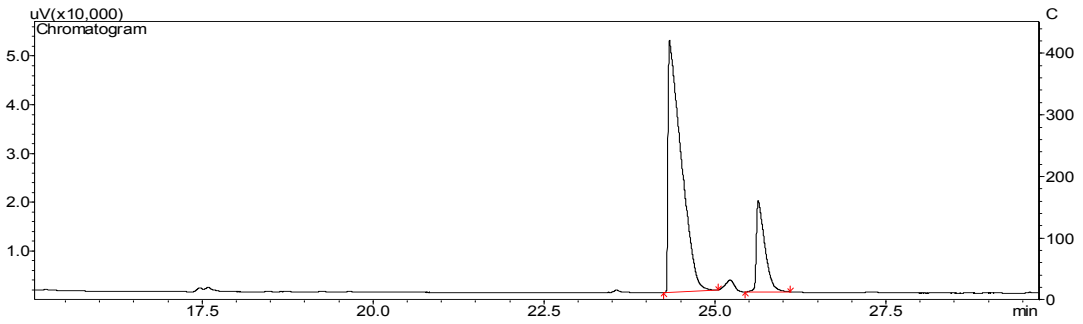

4-methyloxepan-2-one (7); 6-methyloxepan-2-one (8) 60°C, 1°C/min 80°C, 4°C/min 170°C,
t_r (S, 7) = 32.846 min, t_r (*R*, 7) = 33.092 min,
t_r (*R*, 8) = 33.341 min, t_r (*S*, 8) = 33.633 min.

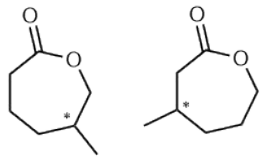

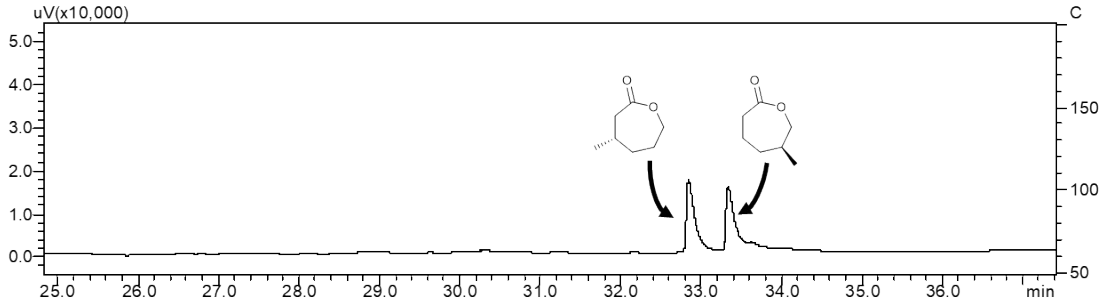

REFERENCES

1 (*a*) I. Polyak, M. T. Reetz and W. Thiel, *J. Am. Chem. Soc.*, 2012, **134**, 2732-2741; (*b*) I. Polyak, M. T. Reetz and W. Thiel, *J. Phys. Chem. B*, 2013, **117**, 4993-5001.

2 (*a*) R. Huey, G. M. Morris, A. J. Olson and D. S. Goodsell, *J. Comput. Chem.*, 2007, **28**, 1145-1152; (*b*) G. M. Morris, D. S. Goodsell, R.S. Halliday, R. Huey, W. E. Hart, R. K. Belew and A. J. Olson, *J. Comput. Chem.*, 1998, **19**, 1639-1662.

3 Gaussian 09, Revision A.01, M. J. Frisch, G. W. Trucks, H. B. Schlegel, G. E. Scuseria, M. A. Robb, J. R. Cheeseman, G. Scalmani, V. Barone, B. Mennucci, G. A. Petersson, H. Nakatsuji, M. Caricato, X. Li, H. P. Hratchian, A. F. Izmaylov, J. Bloino, G. Zheng, J. L. Sonnenberg, M. Hada, M. Ehara, K. Toyota, R. Fukuda, J. Hasegawa, M. Ishida, T. Nakajima, Y. Honda, O. Kitao, H. Nakai, T. Vreven, J. A. Montgomery, Jr., J. E. Peralta, F. Ogliaro, M. Bearpark, J. J. Heyd, E. Brothers, K. N. Kudin, V. N. Staroverov, R. Kobayashi, J. Normand, K. Raghavachari, A. Rendell, J. C. Burant, S. S. Iyengar, J. Tomasi, M. Cossi, N. Rega, J. M. Millam, M. Klene, J. E. Knox, J. B. Cross, V. Bakken, C. Adamo, J. Jaramillo, R. Gomperts, R. E. Stratmann, O. Yazyev, A. J. Austin, R. Cammi, C. Pomelli, J. W. Ochterski, R. L. Martin, K. Morokuma, V. G. Zakrzewski, G. A. Voth, P. Salvador, J. J. Dannenberg, S. Dapprich, A. D. Daniels, Ö. Farkas, J. B. Foresman, J. V. Ortiz, J. Cioslowski, and D. J. Fox, Gaussian, Inc., Wallingford CT, 2009

4 (*a*) C. Lee, W. Yang and R. G. Parr, *Phys. Rev. B*, 1988, **37**, 785–789; (*b*) A. D. Becke, *J. Chem. Phys.*, 1993, **98**, 5648-5652.

5 C. I. Bayly, P. Cieplak, W. Cornell and P. A. Kollman, *J. Phys. Chem*., 1993, **97**, 10269-10280.

6 D.A. Case, J.T. Berryman, R.M. Betz, D.S. Cerutti, T.E. Cheatham, III, T.A. Darden, R.E. Duke, T.J. Giese, H. Gohlke, A.W. Goetz, N. Homeyer, S. Izadi, P. Janowski, J. Kaus, A. Kovalenko, T.S. Lee, S. LeGrand, P. Li, T. Luchko, R. Luo, B. Madej, K.M. Merz, G. Monard, P. Needham, H. Nguyen, H.T. Nguyen, I. Omelyan, A. Onufriev, D.R. Roe, A. Roitberg, R. Salomon-Ferrer, C.L. Simmerling, W. Smith, J. Swails, R.C. Walker, J. Wang, R.M. Wolf, X. Wu, D.M. York and P.A. Kollman, AMBER 2015, University of California, San Francisco, CA, 2015.

7 V. Hornak, R. Abel, A. Okur, B. Strockbine, A. Roitberg and C. Simmerling, *Proteins*, 2006, **65**, 712-725.

8 J. Wang, R. M. Wolf, J. W. Caldwell, P. A. Kollman and D. A. Case, *J. Comput. Chem*., 2004, **25**, 1157-1174.

9 T. Darden, D. York and L. Pedersen, *J. Chem. Phys.*, 1993, **98**, 10089-10092.

10 J.-P. Ryckaert, G. Ciccotti and H. J. C. Berendsen, *J. Comput. Phys.*, 1977, **23**, 327-341.

11 G. Chen, M. M. Kayser, M. D. Mihovilovic, M. E. Mrstik, C. A. Martinez and J. D. Stewart, *New J. Chem*., 1999, **23**, 827-832.

12 M. J. Taschner, D. J. Black; Q. Z. Chen, *Tetrahedron: Asymmetry*, 1993, **4**, 1387-1390.

13 V. Alphand, R. Furstoss, S. M. Pedragosa, S. M.Roberts, and A. J.Willetts, *J. Chem. Soc., Perkin Trans. I*, 1996, **15**, 1867-1872.

14 S. Wang, M. M. Kayser, V. Jurkauskas, *J. Org. Chem.* 2003, **68**, 6222–6228.